Aspect Ratios of Airborne Dust

Ping Yang[1] (PI) and K.-N. Liou[2] (Co-I)
Xin Huang[1]

1.Texas A&M University
2.University of California, Los Angeles

Outline

- Motivation
- Readiness of datasets and modeling capabilities
- Some preliminary results
- Summary

博联社

中新網圖
chinanews.com

拯救民勤
www.minqin.cn

库尔勒
三十六团
cnsphoto

Airborne dust originating with small-scale sources may undergo large-scale transport

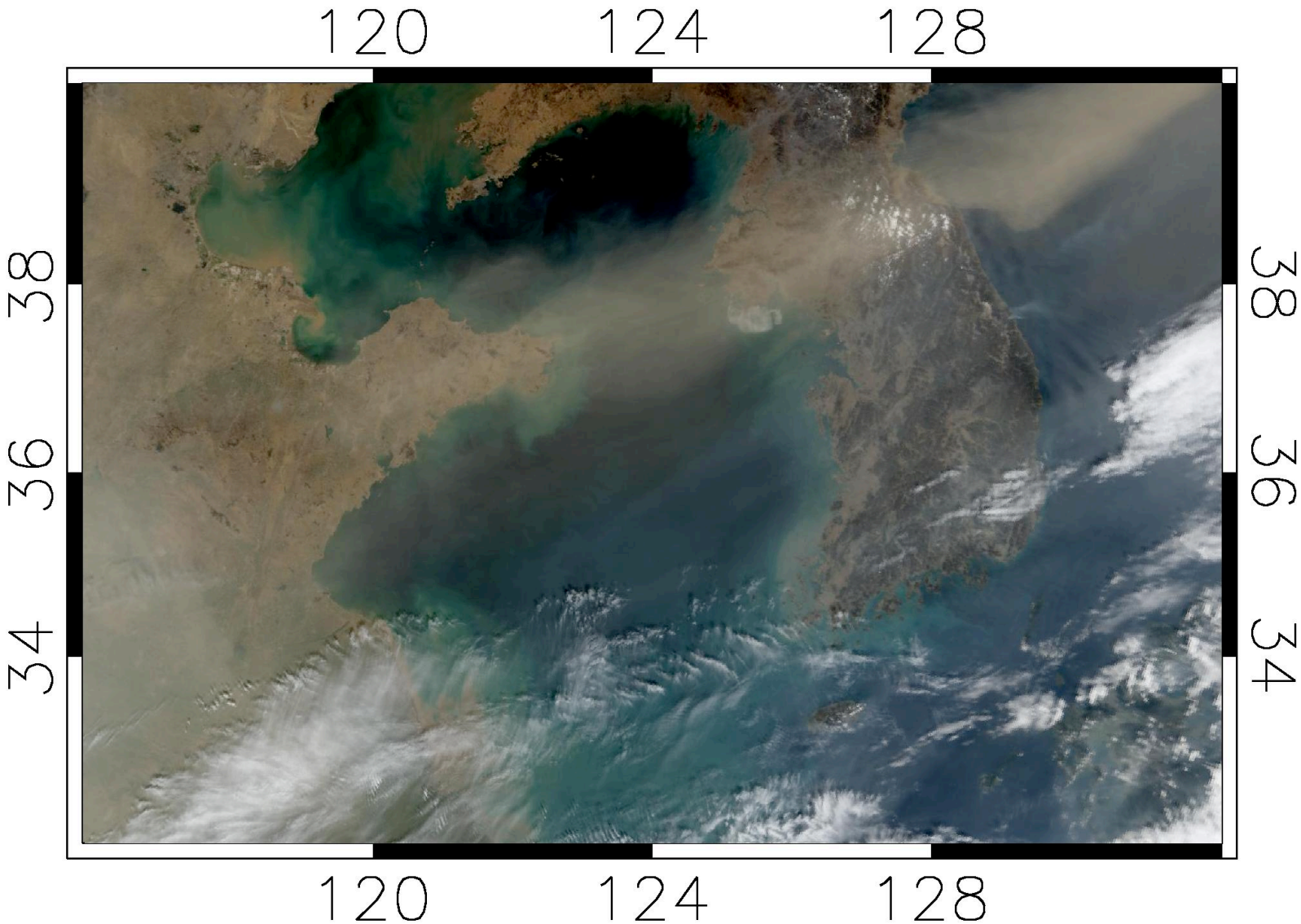

Asian Dust, MODIS RGB (0.65µm, 0.55µm, 0.47µm) Image

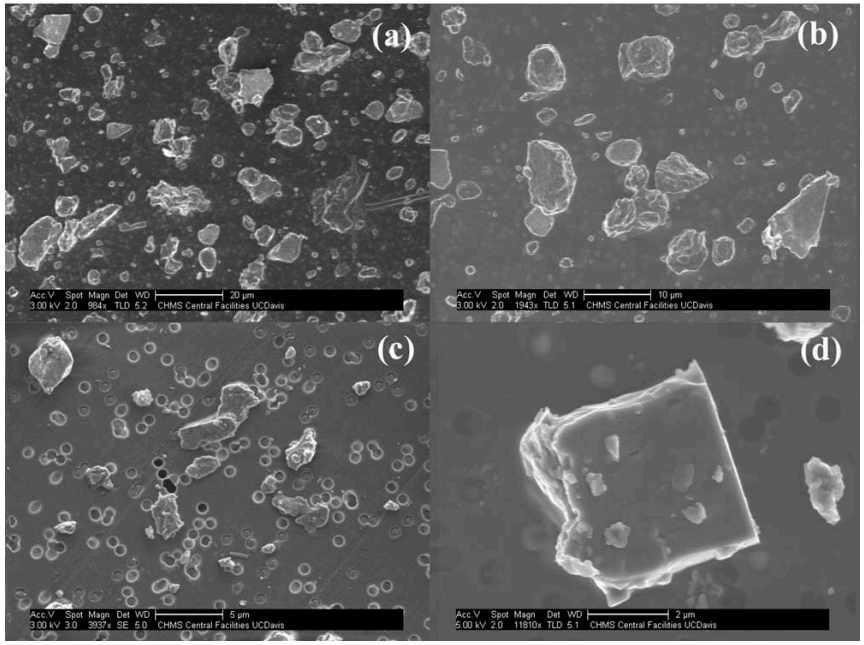

Reid et al., 2003

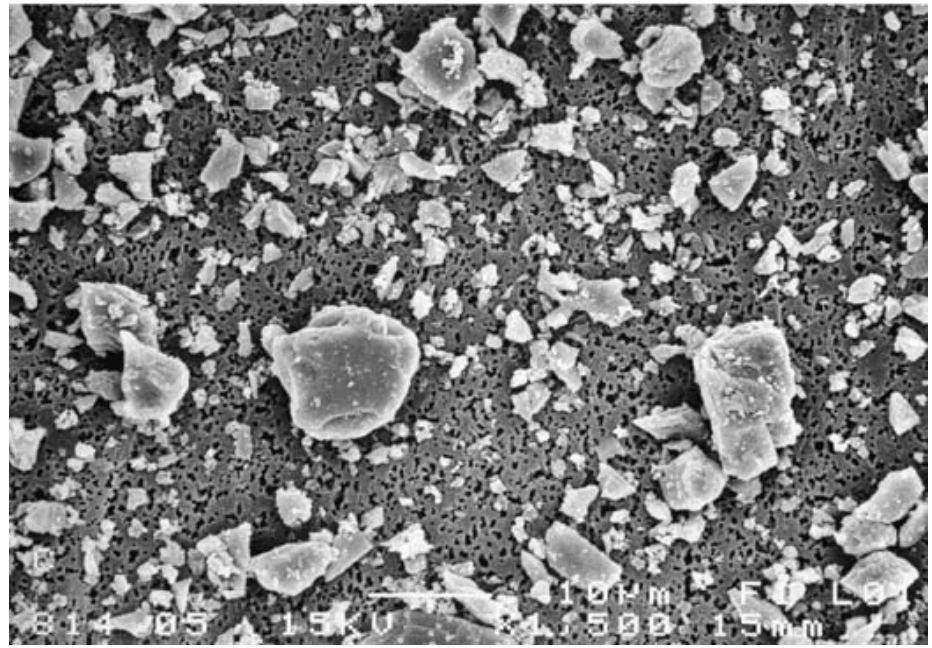

Volten et al., 2005

Nonsphericity Effect of Dust Particles

- "…even moderate nonsphericity results in substantial errors in the retrieved aerosol optical thickness if satellite reflectance measurements are analyzed using Mie theory" (Mishchenko et al. 1995).
- "Multiple, multispectral remote sensing observations, such as those anticipated from the Earth Observing System (EOS) multiangle imaging spectroradiometer (MISR), can distiguish spherical and nonspherical particles over calm ocean for mineral-dust-like particles" (Kahn et al. 1997).
- Demonstrated importance of the impact of dust particle's nosnphericity on the retrieval of dust microphysical and optical properties (Dubovik et al. 2002, 2006)

Simulated solar reflectance at the top of a dusty atmosphere. Spherical and nonspherical (spheroidal) shapes are assumed for dust particles (Yang, Feng, Hong, Kattawar, Wiscombe, Mishchenko, Dubovik, Laszlo, and Sokolik, 2007).

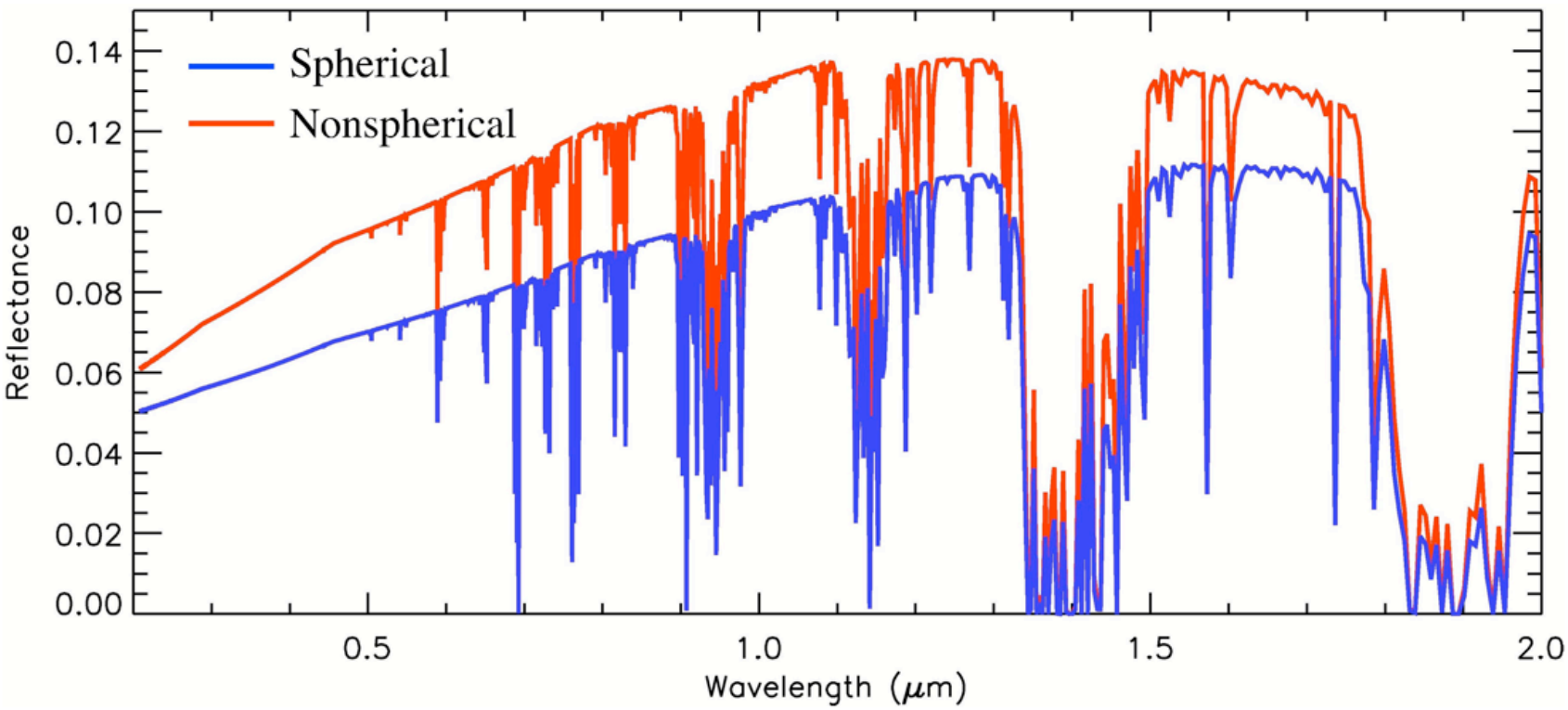

- These results indicate that the equivalent sphere approximation leads to an underestimate of the albedo of a dusty atmosphere. This underestimate has an important implication to the study of the effect of airborne dust on the radiation budget within the atmosphere.

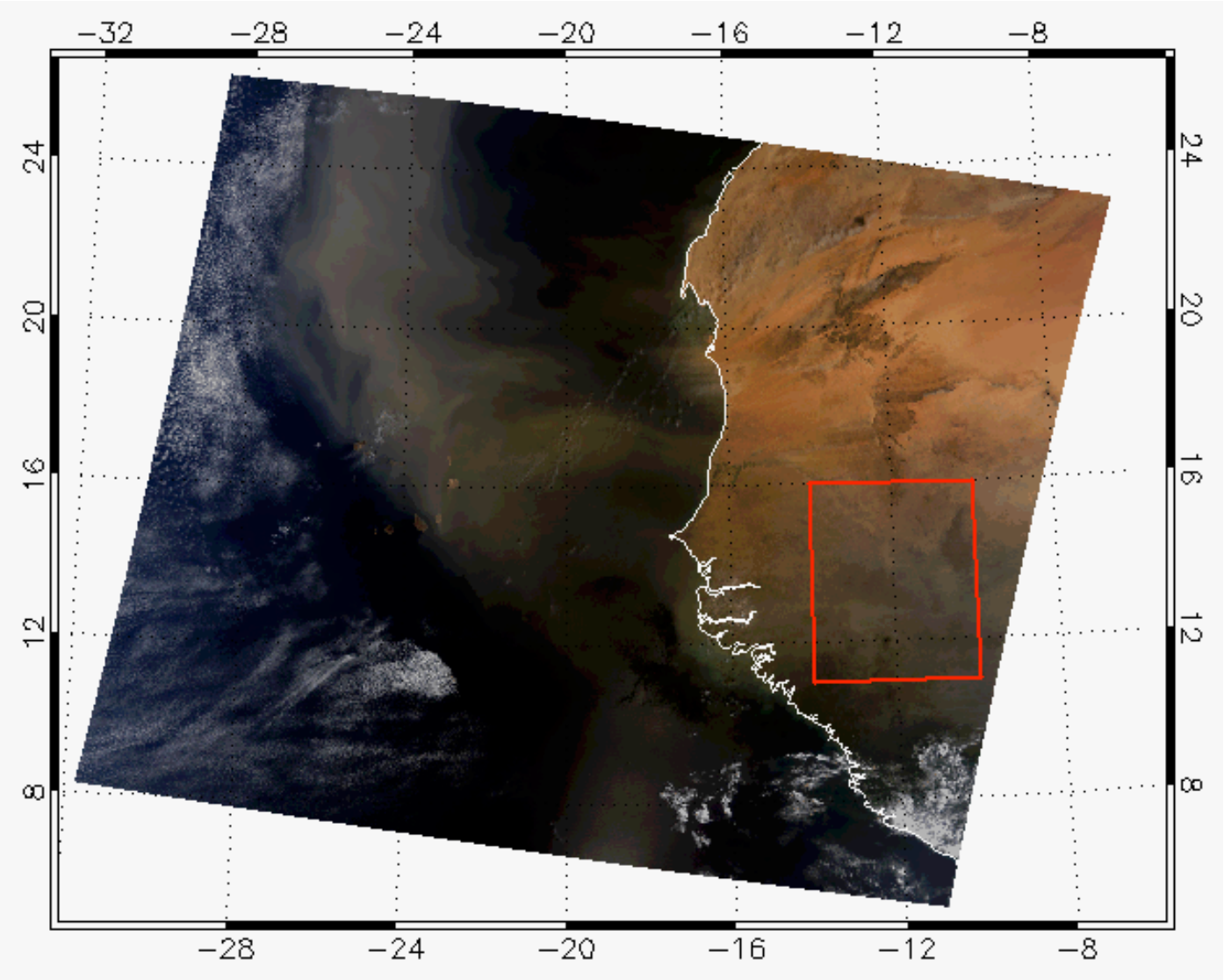

MODIS RGB image on March 2, 2003, showing a dust plume over West Africa. The area indicated by the small red box is used to retrieve dust AOD in the present sensitivity study (Feng, Yang, Kattawar, Hsu, Tsay and Laszlo, 2009).

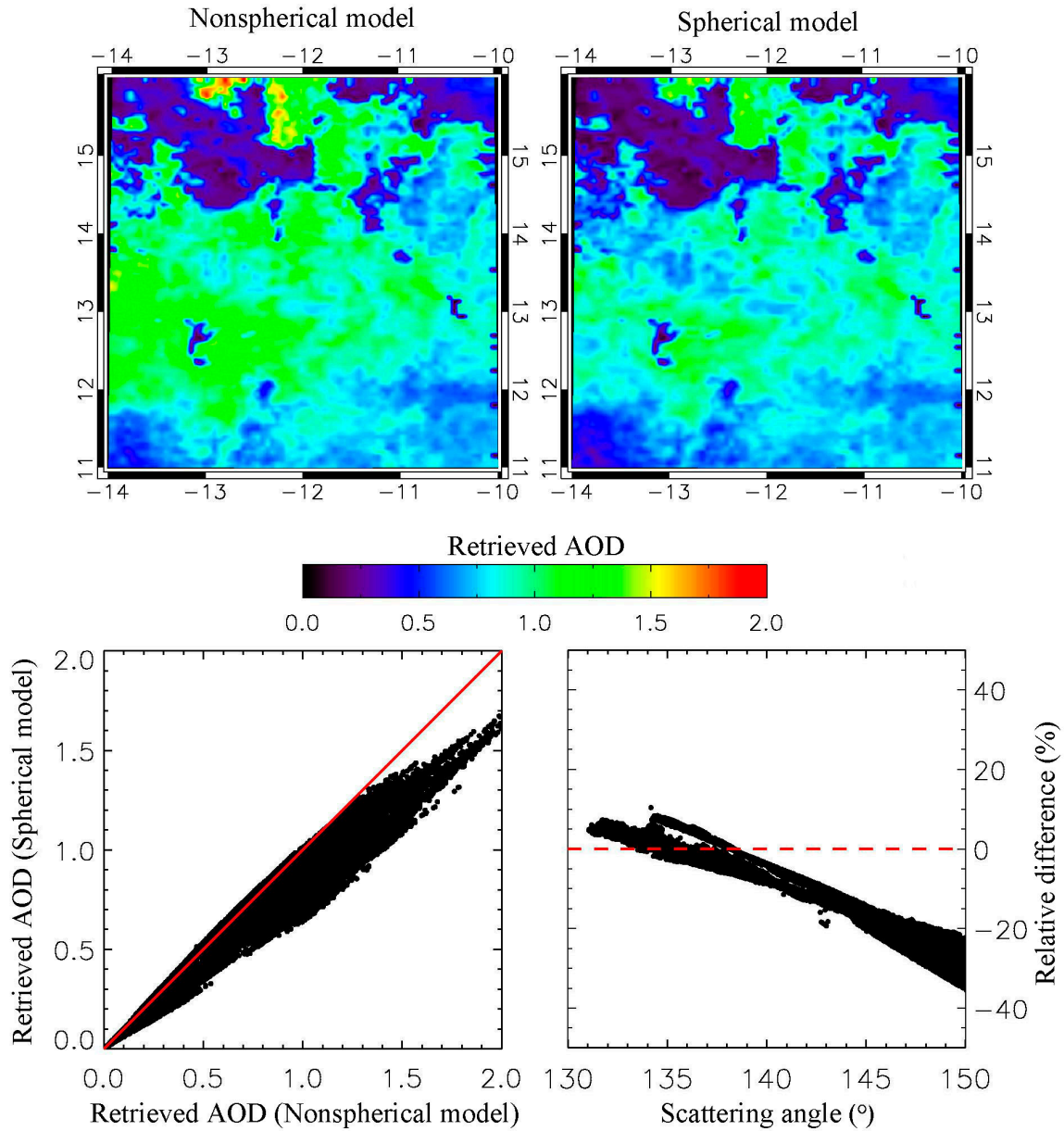

Upper panels: the retrieved dust AOD based on the nonspherical (spheroidal) and sphere models.

Lower left panel: retrieved dust AOD based on the sphere model versus those based on the nonspherical model.

Lower right panel: the relative differences of the retrieved AOD (Feng, Yang, Kattawar, Hsu, Tsay and Laszlo, 2009).

MODIS RGB image (05/27/2008)

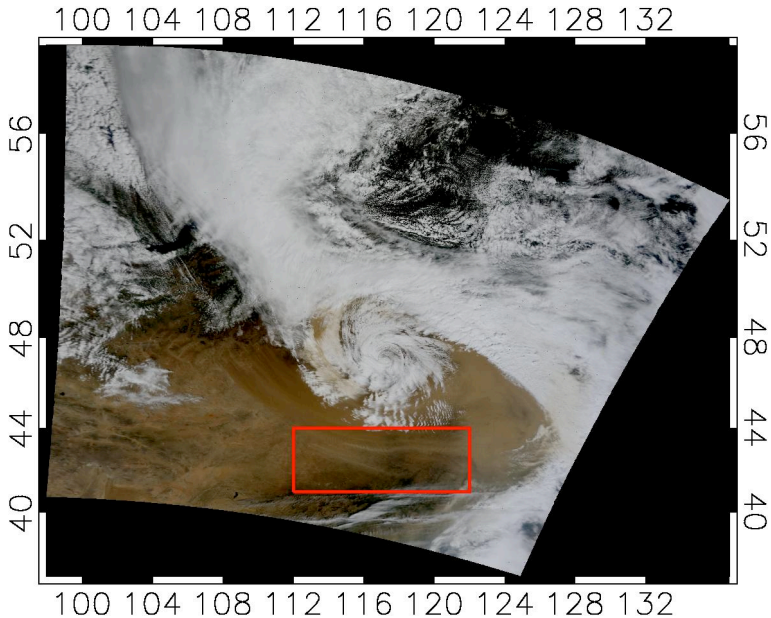

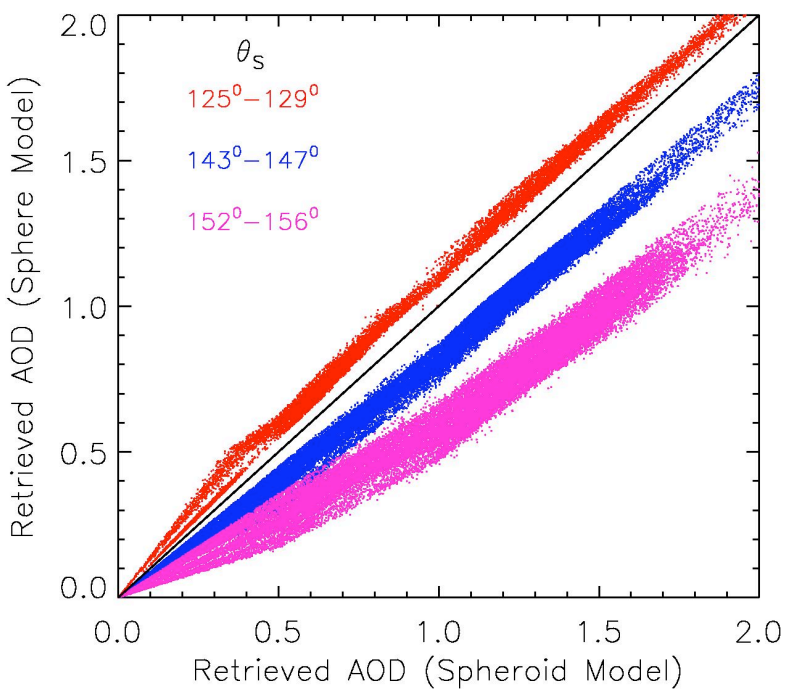

Retrieved dust optical depths

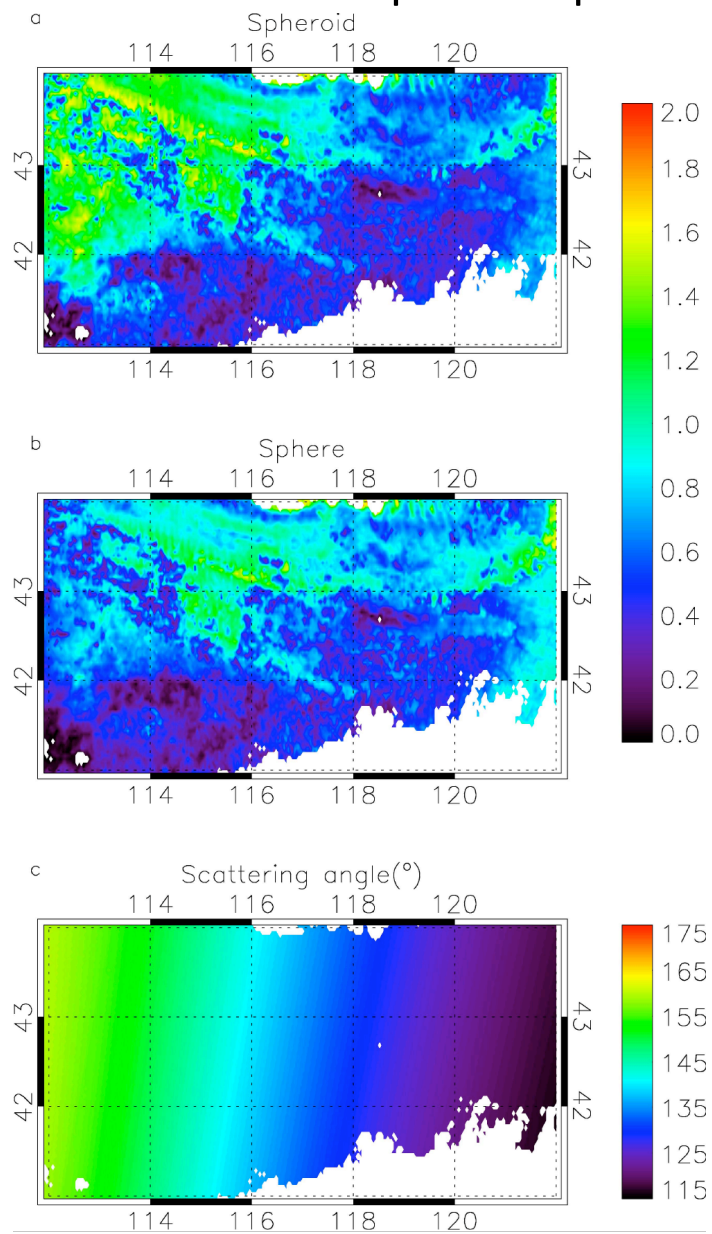

(Q. Feng, Texas A&M Univ)

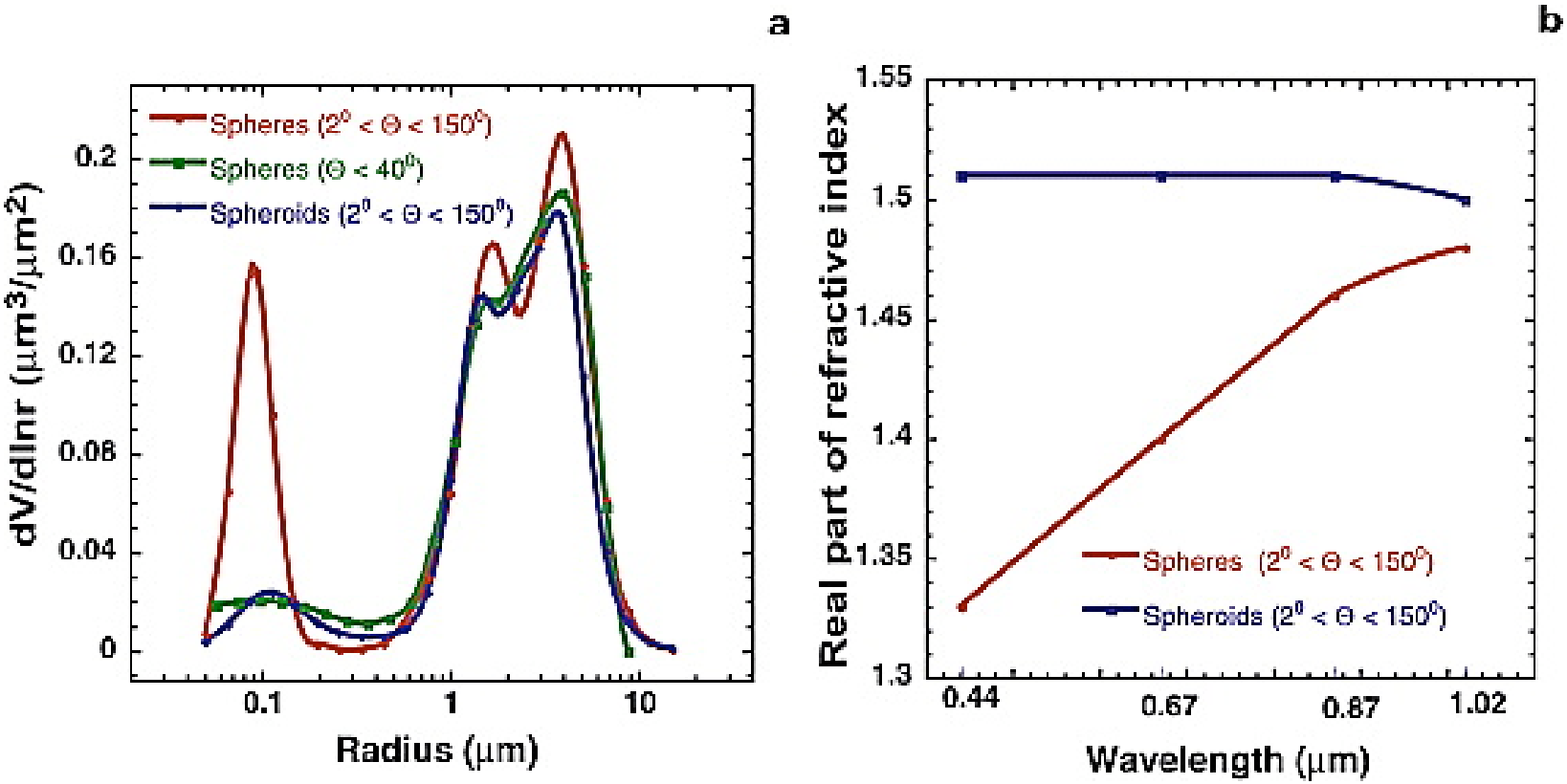

A typical situation where utilizing the spheroid scattering assumption [*Dubovik et al.*, 2002b] resulted in the removal of the false fine mode in the size distribution and false spectral dependence in the real part of refractive index. Size distributions and refractive indices are retrieved assuming sphere and spheroid models from spectral radiance measurements covering the full range of scattering angles. The size distribution retrieved from the aureole only (Θ < 40°, where effects of nonsphericity are minimal) and assuming spherical particles is also shown. *Adapted from Dubovik et al. (2006).*

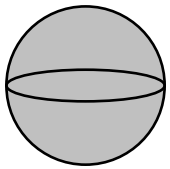

Kaufman et al., 1994

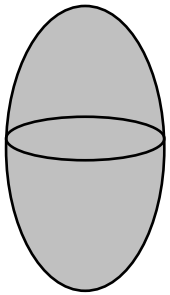

Mishchenko et al., 1997

Dubovik et al., 2006

Yang et al., 2007

Many others

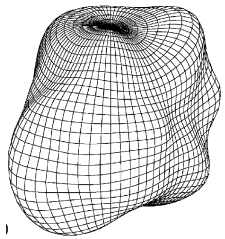

Nousiainen et al., 2003; Sun et al. 2003; Nousiainen and Muinonen, 2007

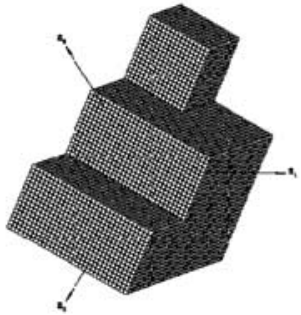

Kalashnikova and Sokolik, 2004

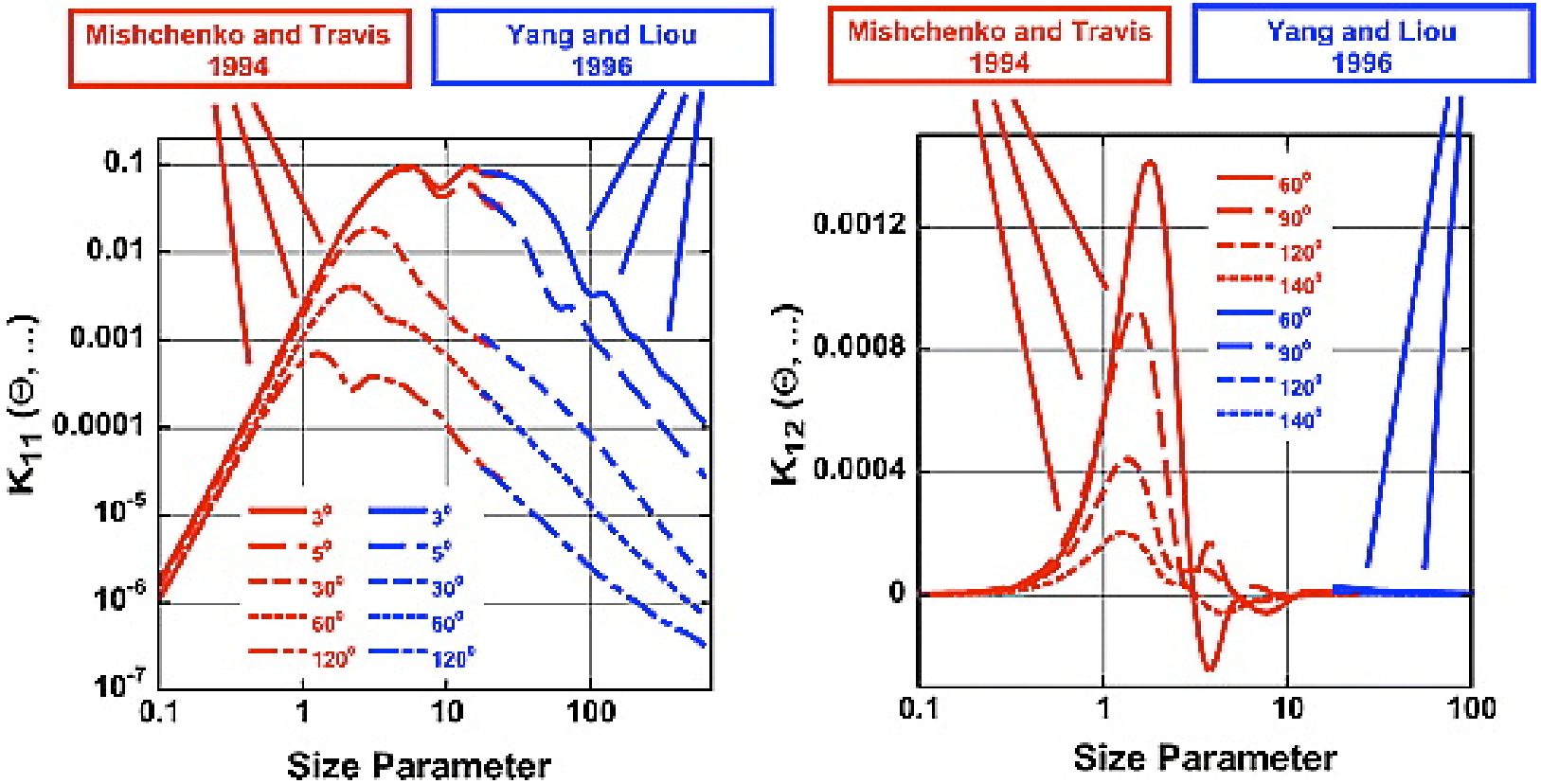

Elements of the kernel matrices $K_{11}(\Theta, \lambda, n, k, p, rk)$ and $K_{12}(\Theta, \lambda, n, k, p, rk)$ at different scattering angles for prolate randomly oriented spheroids (ε= ~2.7, n = 1.53+i0.003). The red and blue curves show the results obtained with the *T*-matrix code [*Mishchenko and Travis*, 1994] and the *Yang and Liou* [1996] method, respectively. *Adapted from Dubovik et al. (2006),*

New Effort

- Objective

  Use manageable and "optimal" particle morphological sets (or, the geometric parameters associated with particle shapes and compositions) to quantify the effect of the nonsphericity of dust particles on their optical and radiative properties from remote sensing and radiative forcing perspectives.

- Particle shapes

  Tri-axial ellipsoid (Bi, Yang, Kattawar, and Kahn, 2008)

  Non-symmetric hexahedra (Bi, Yang, Kattawar, and Kahn, 2010)

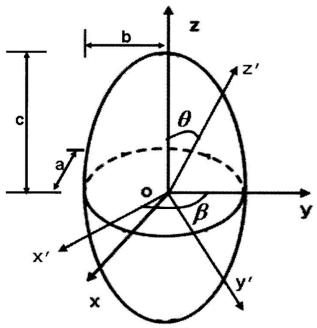

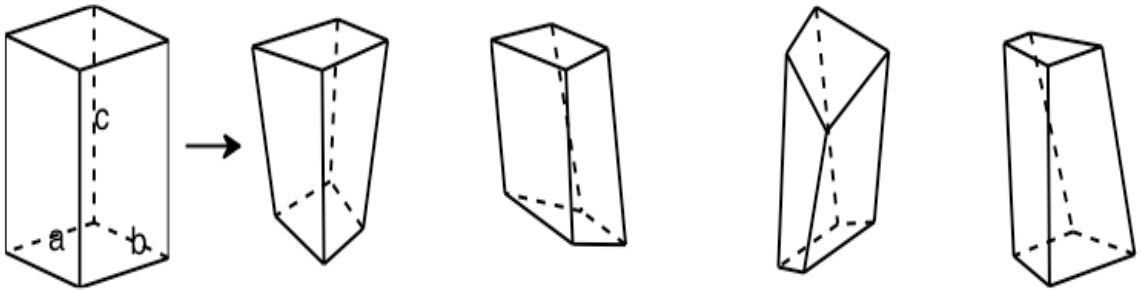

HEXAHEDRA, PHASE MATRIX ELEMENTS

(Bi, Yang, Kattawar, and Kahn, 2010)

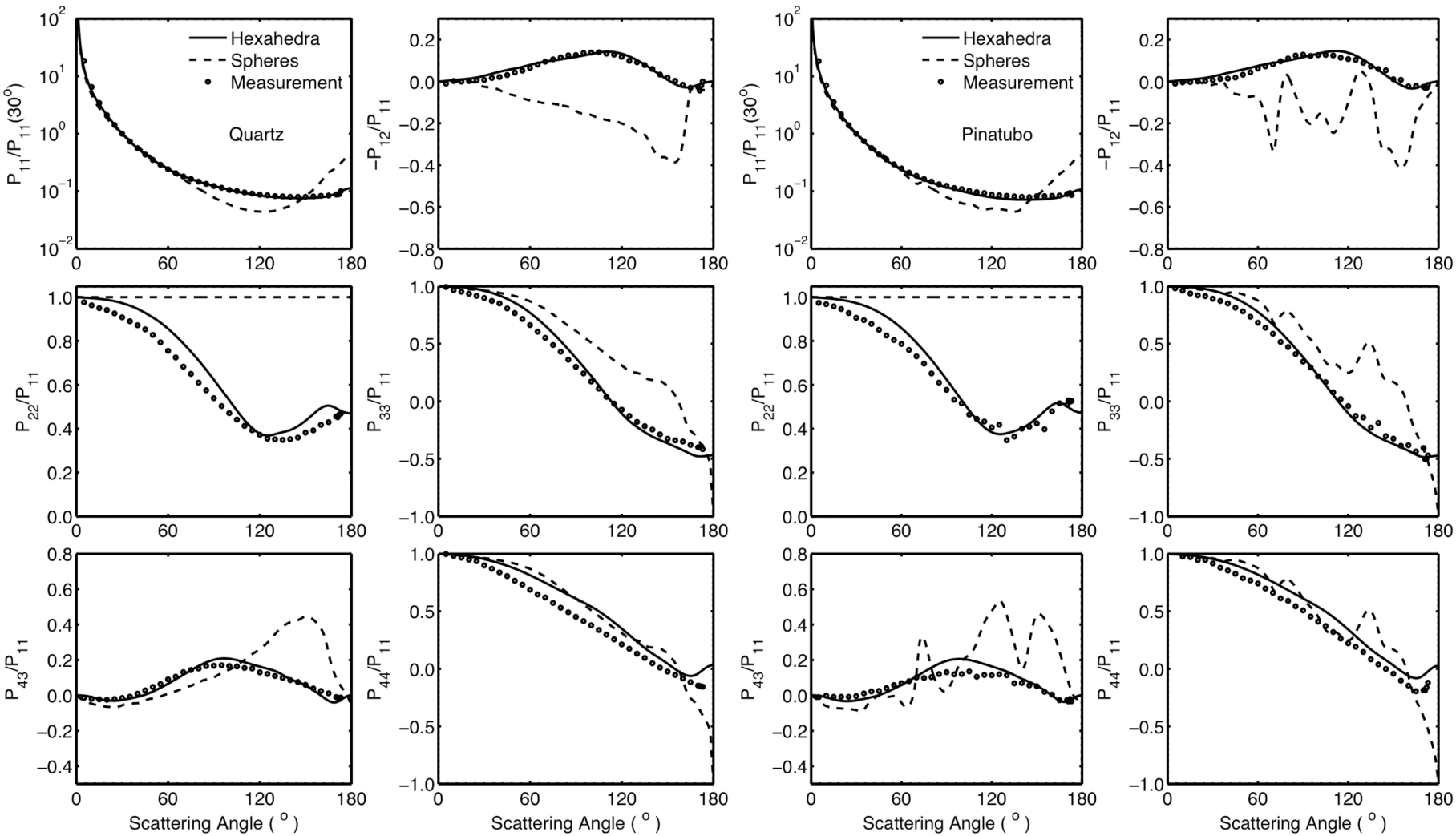

Effective radius r_e= 2.3 μm, variance =1.5

Effective radius r_e= 3 μm, variance =12.3

Database

Meng, Z., P. Yang, G. W. Kattawar, L. Bi, K. N. Liou, I. Laszlo, 2010: Single -scattering Properties of Tri-axial Ellipsoidal Mineral Dust Aerosols: A Database for Application to Radiative Transfer Calculations, *J. of Aerosol Science, 41, 501-512.*

The selection of refractive index:

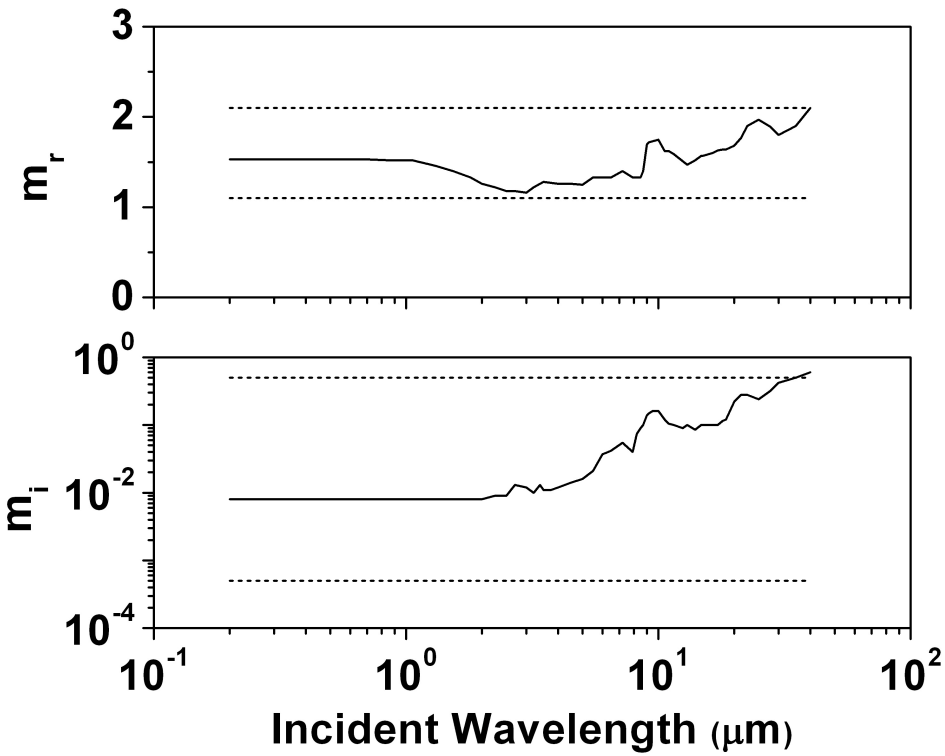

Complex refractive indices of dust and the simulation domain (the area between two dashed lines). Data are taken from Levoni et al. (1997)

$$1.10 \le m_r \le 2.10$$

$$0.0005 \le m_i \le 0.5000$$

In this database:

- The relation between wavelength and dust refractive index is NOT fixed.
- Size Parameter ($x=2\pi c/\lambda$): $0.025 \le x \le 1000$
- 42 aspect ratios

Bulk scattering phase functions and the weight of different aspect ratios

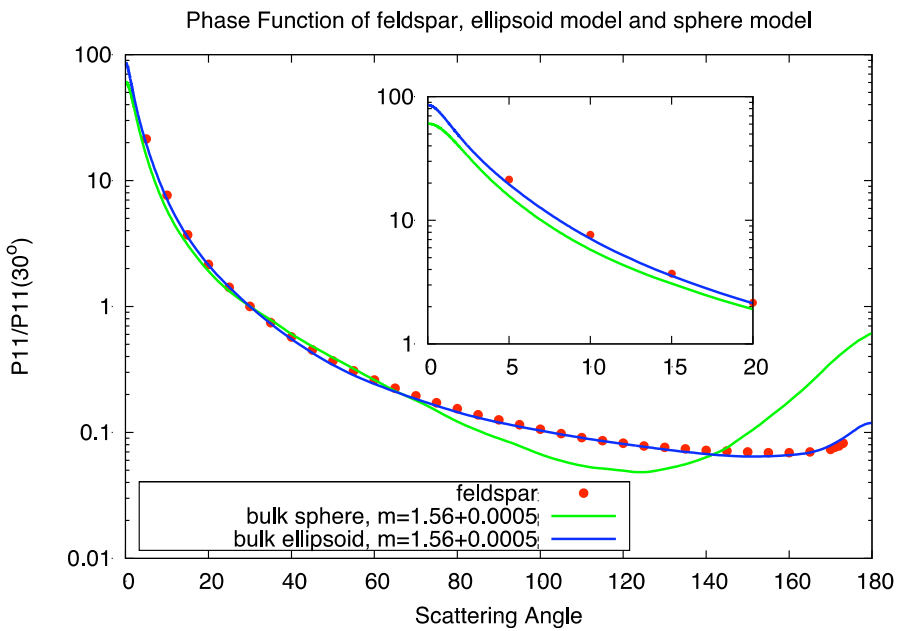

The weight W_k is determined by the **Monte Carlo method** to minimize the difference between the logarithm of the bulk ellipsoid phase function and the observed phase function of feldspar.

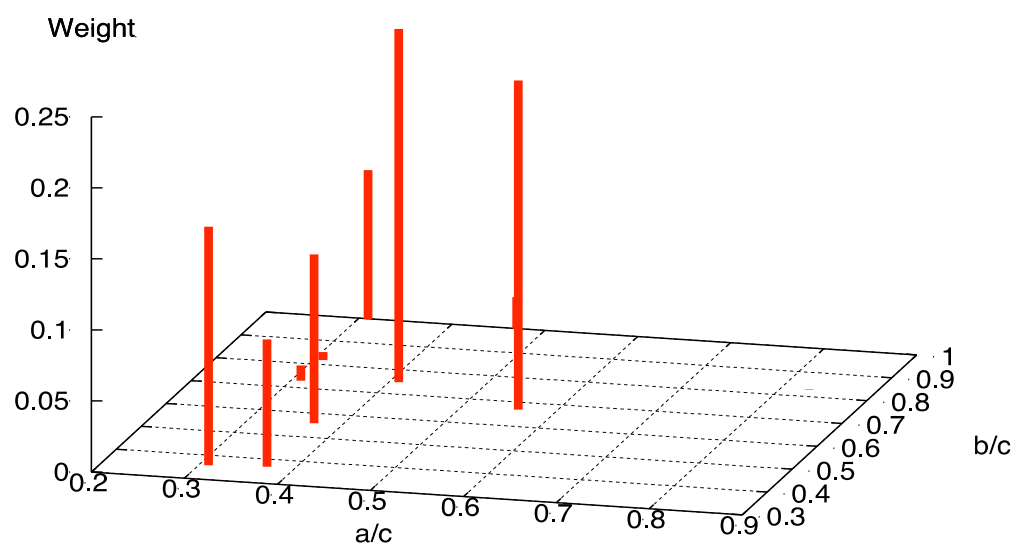

The mean aspect ratio of bulk ellipsoid mixture is :

a/c = 0.409, b/c = 0.641

Yi, Hsu, Yang, Tsay, J. Aerosol Sci., (2011)

Integrated net flux of dust forcing at the top of the atmosphere (TOA) and the surface using the spherical and nonspherical models under various conditions

(Solar spectral band: 0.3μm-4.5μm)

Conditions		Integrated Dust Forcing (W/m^2)			
Surface type	Optical depth	TOA		Surface	
		Nonspherical	Difference	Nonspherical	Difference
Sandy	0.5	-1.1	6.1	-71.0	6.3
Sandy	1.0	-3.5	10.9	-136.6	11.0
Water	0.5	-26.7	8.7	-90.1	9.1
Water	1.0	-48.2	14.7	-170.9	15.4

Difference = the nonspherical results minus the spherical counterparts

Yi, Hsu, Yang and Tsay, J. Aerosol Sci., (2011)

Dust non-spherical effect on polarization measurement

- Spherical aerosol may be not sufficient for the multi-angular polarization remote sensing. (J. L. Deuze et al., 2000)

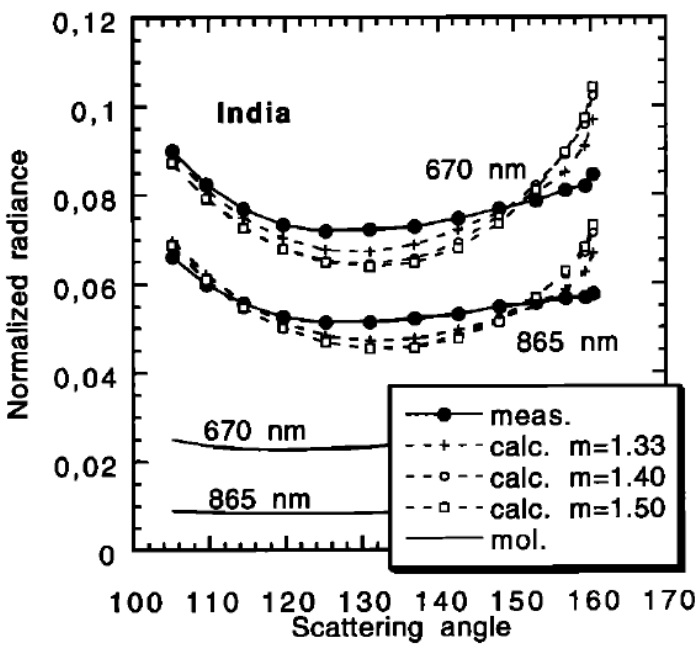

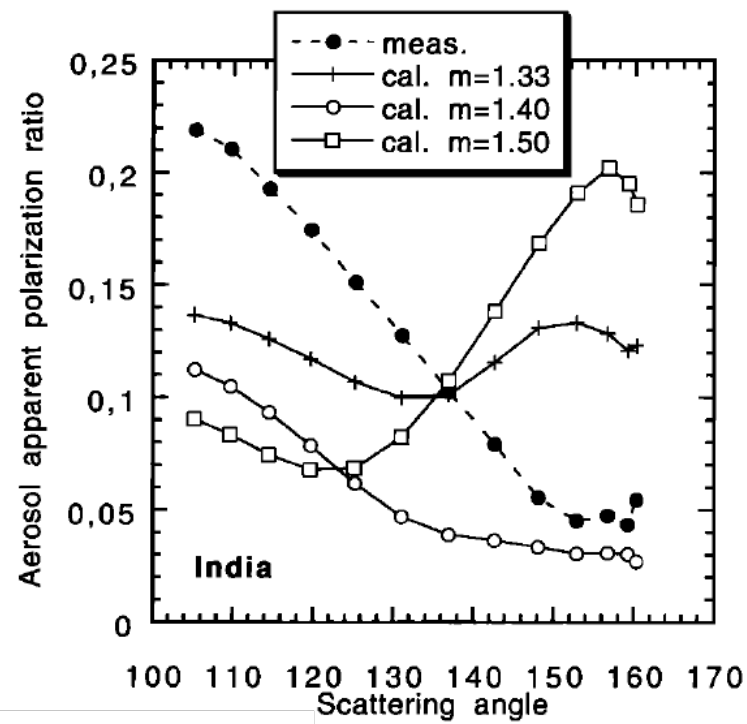

$$P_\lambda^m = \frac{\sqrt{(Q_\lambda^m - Q_\lambda^{\mathrm{mol}})^2 + (U_\lambda^m - U_\lambda^{\mathrm{mol}})^2}}{L_\lambda^m - L_\lambda^{\mathrm{mol}}}$$

POLDER Instrument

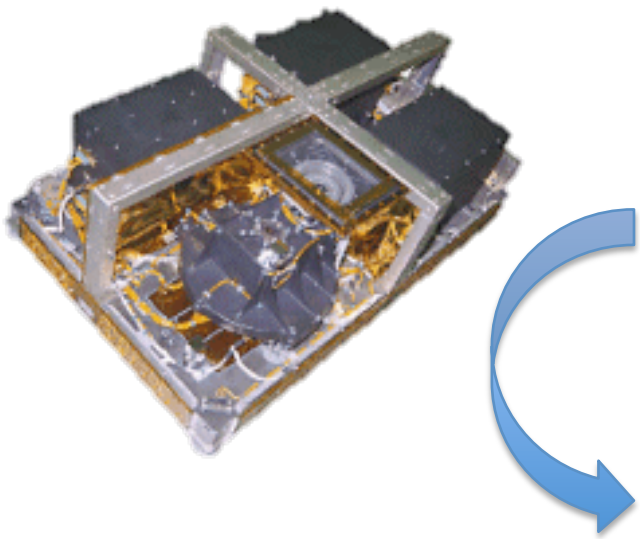

Field of View	102 (across track) by 86 degree (along track)
Swath	2400 km
Resolution of a Pixel	6 by 7 km at nadir
Spectral Range	443 to 910 nm (9 bands)
Time Lapse for All Channels	4.9 s
Multi-polarization	443, 670 and 865 bands are polarized
Multi-directionality	Up to 14 directions per pixel per pass

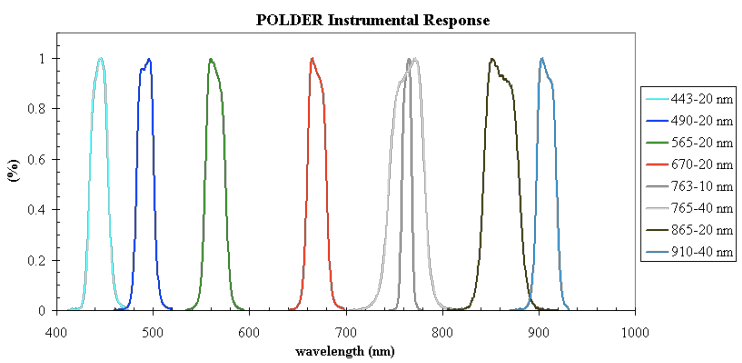

Band	Central Wavelength (nm)	Band Width (nm)	Usage
443P	444.5	20	ocean color
443	444.9	20	aerosol, ERB
490	492.2	20	ocean color
565	564.5	20	ocean color
670P	670.2	20	vegetation, aerosol, ERB
763	763.3	10	cloud top pressure
765	763.1	40	aerosol
865P	860.8	40	vegetation, aerosol, ERB
910	907.7	20	water vapor amount

Fine Mode Oblate Spheroid Aerosol Model for the 865P Band

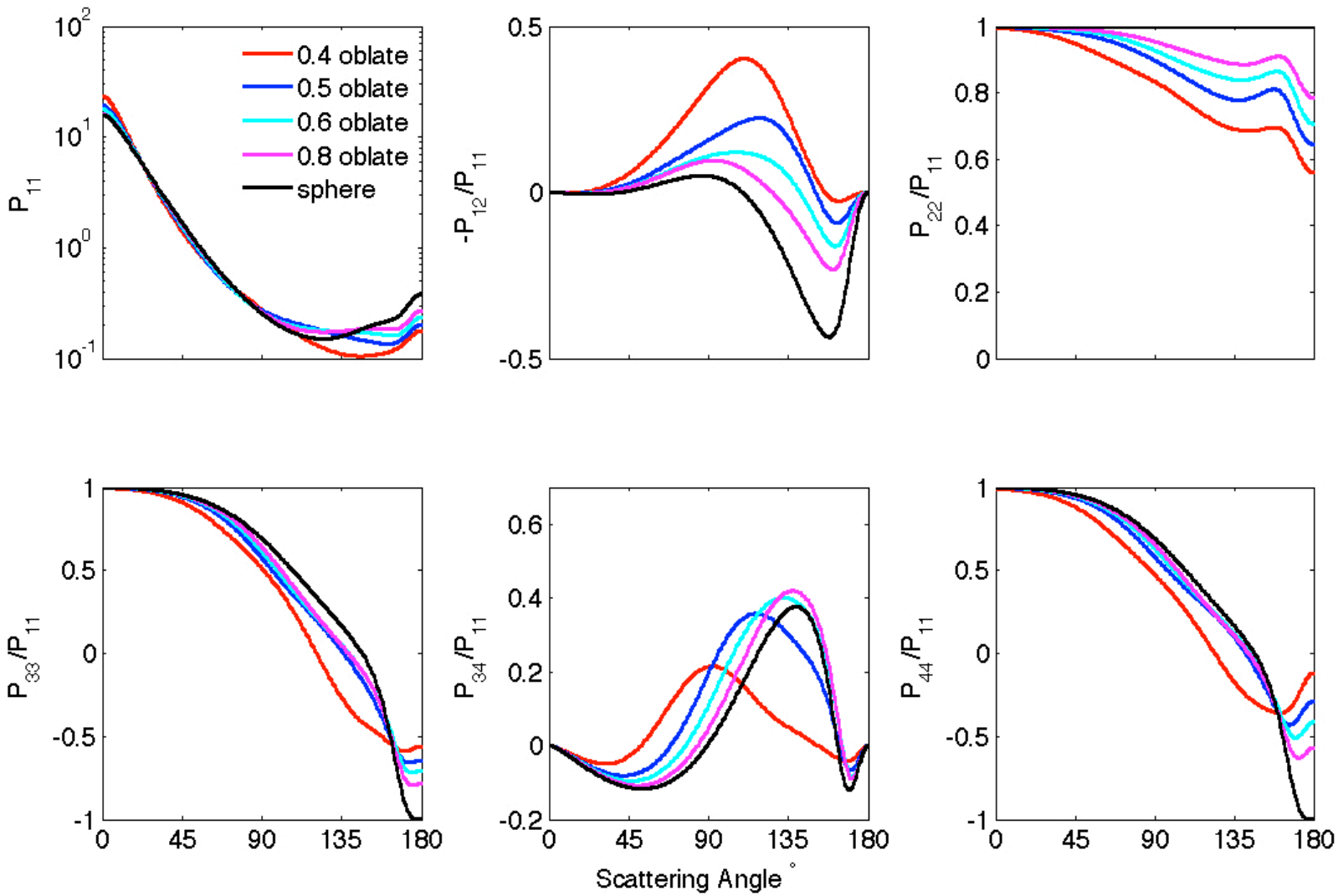

Coarse Mode Prolate Spheroid Aerosol Model for the 865P Band

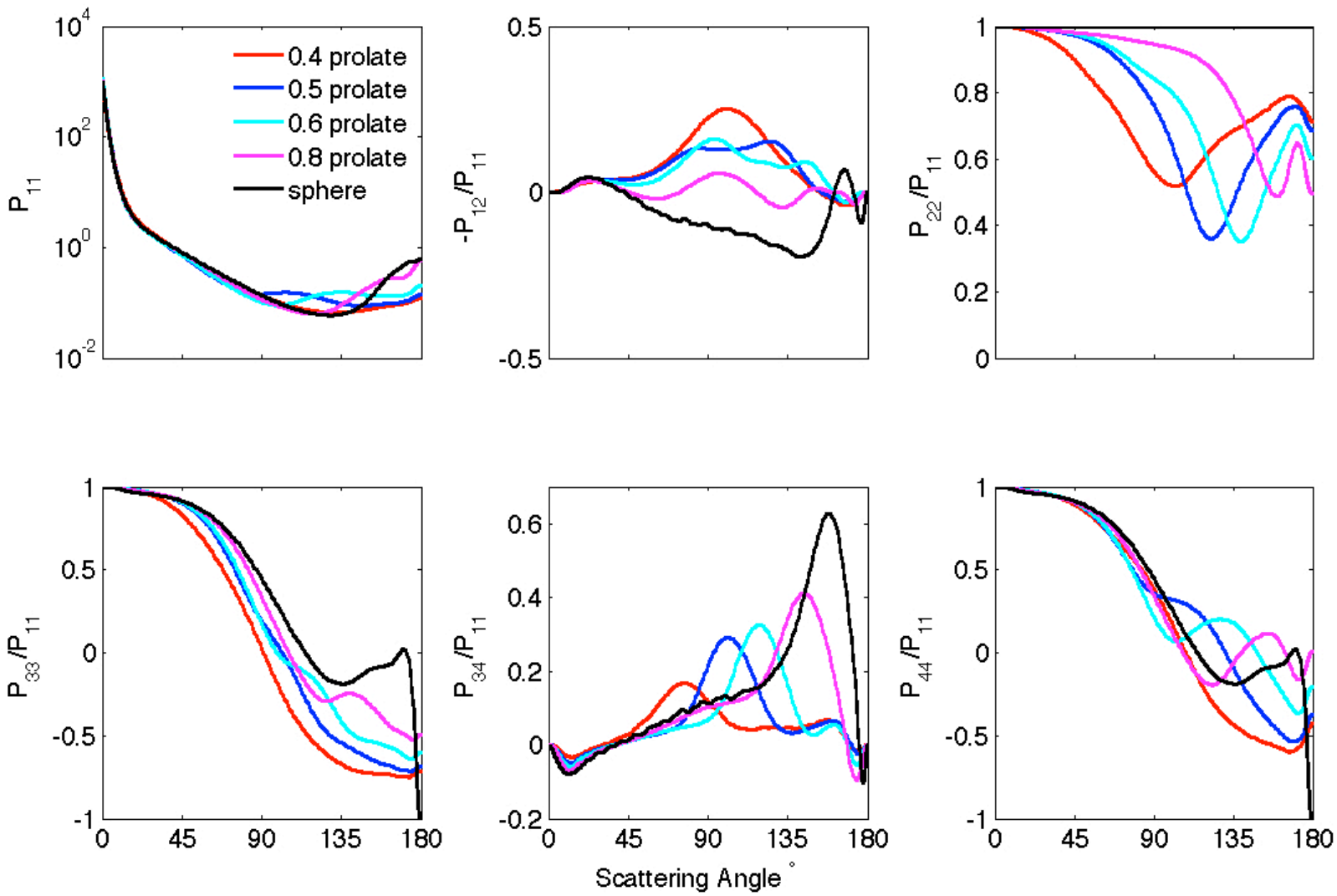

Normalized Radiance and Normalized Polarized Radiance

$$R(\theta_v, \phi_v; \theta_s, \phi_s) = \frac{\pi I(\theta_v, \phi_v; \theta_s, \phi_s)}{E_s}$$

$$R_p(\theta_v, \phi_v; \theta_s, \phi_s) = \mathrm{sgn}\,\frac{\pi\sqrt{Q^2 + U^2}}{E_s}\,\frac{\cos\theta_v + \cos\theta_s}{\cos\theta_s}$$

Laurent C. Labonnote
et al., 2001

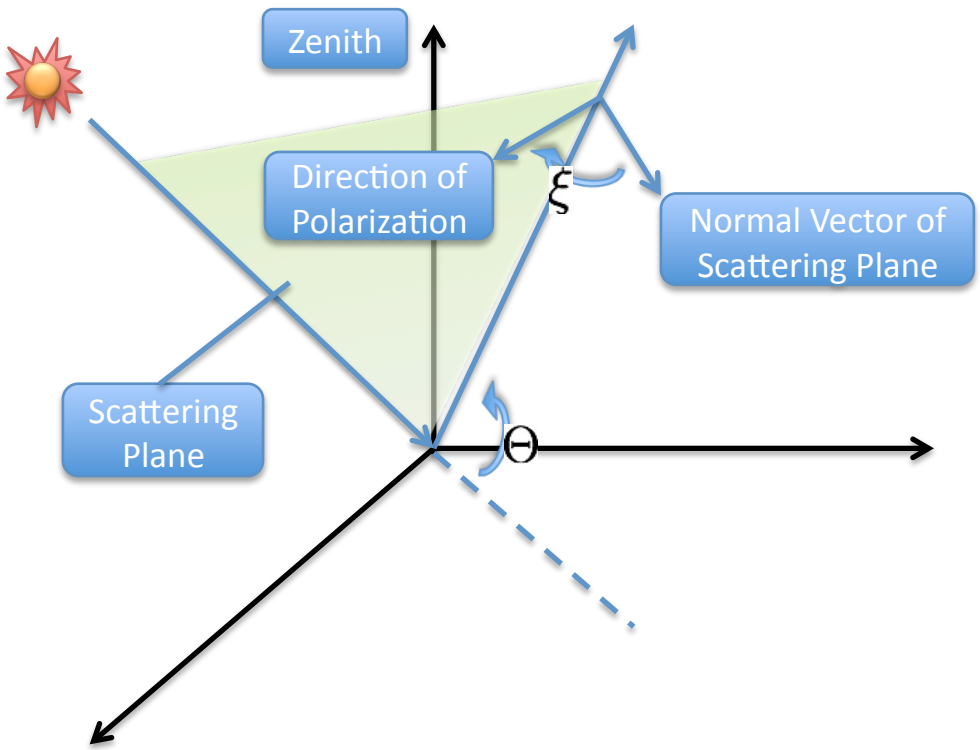

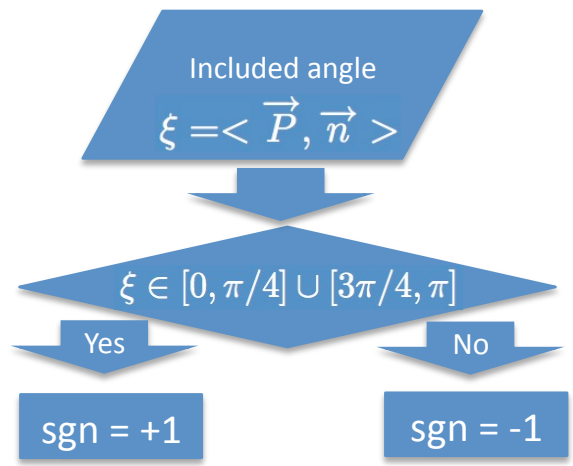

Pixel Selection

	Condition
Surface type	Over global oceans
Cloud detection	Clear sky
Latitude	< 50°
Number of directions within a pixel	> 7
Maximum scattering angle – minimum scattering angle	> 50°

11,347 pixels, up to 158,858 directions are selected on Oct. 1st, 2010
3242 dusty pixels, up to 45,388 directions are selected on April 1st, 2010

Polarization for Clear Sky over Ocean

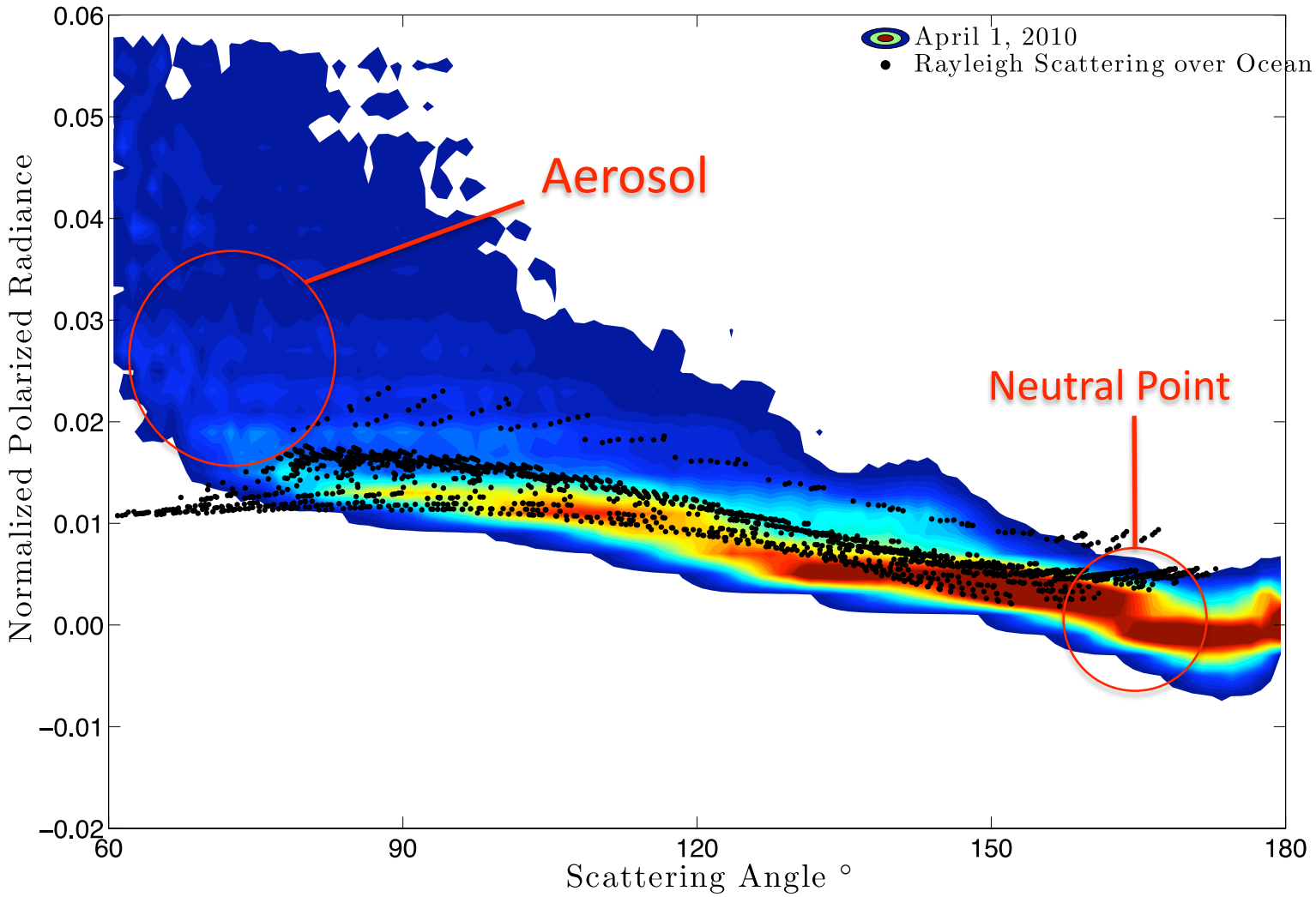

Detection of optically thin mineral dust aerosol layers

- New dust detection algorithm (daytime over ocean)
  - Training data sets: Version 3, 2008 CALIPSO products with MODIS data
    - Three CALIPSO categories: Clear($R_{0.55\mu m}$<0.05), Cloud, Dust
    - No snow/ice, No sunglint
  - Discriminant Analysis

Linear Discriminant Analysis (LDA):
- same covariance matrixe for each groups

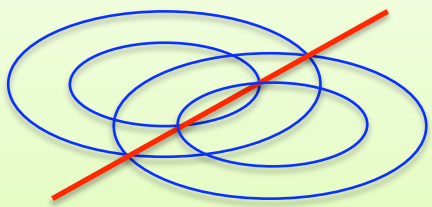

Linear division of the sample space

Quadratic Discriminant Analysis (QDA):
- different covariance matrixes for each groups

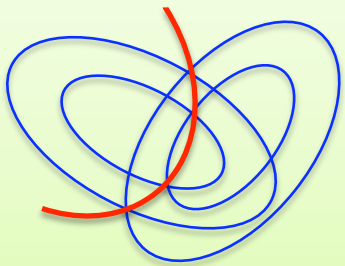

Quadratic division of the sample space

$NDVI[(R_{0.86\mu m}-R_{0.64\mu m})/(R_{0.86\mu m}+R_{0.64\mu m})]$, $NDDI[(R_{2.13\mu m}-R_{0.47\mu m})/(R_{2.13\mu m}+R_{0.47\mu m})]$,
$STD3[R_{0.55\mu m}]$, $R_{0.47\mu m}/R_{0.64\mu m}$, $BTD_{8.5\text{-}11\mu m}$, $BTD_{11\text{-}12\mu m}$

- lookup tables of covariance matrixes, means and prior probabilities
  six latitude bands (-90~-60, -60~-30, -30~0, 0~30, 30~60, and 60~90)
  four seasons (MAM, JJA, SON, DJF)

H.-M. Cho, Texas A&M Univ.

Detection of optically thin mineral dust aerosol layers

- Case study (April 2, 2008 1450UTC)

MODIS RGB image with CALIPSO track

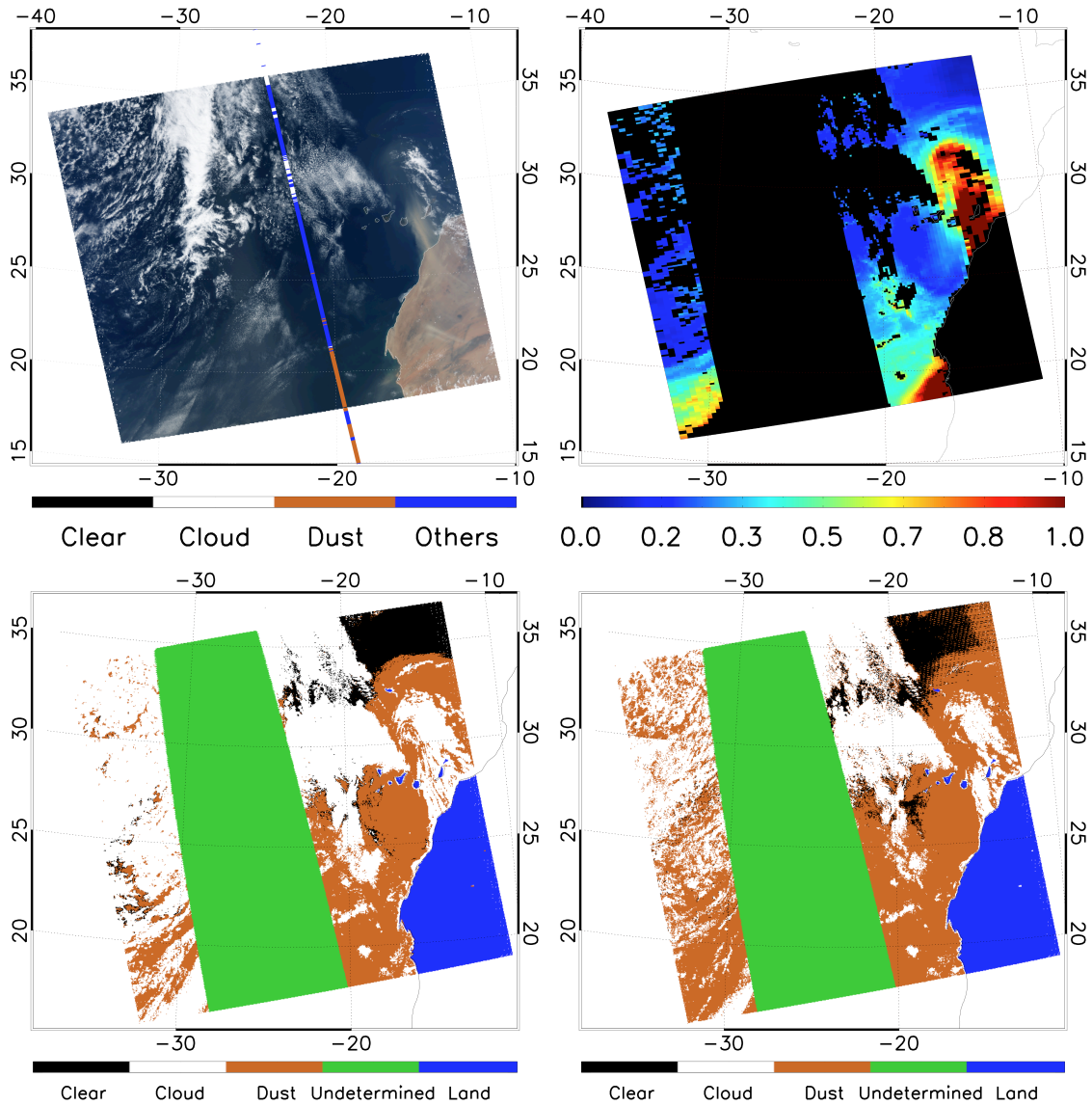

MODIS AOT

LDA

QDA

H.-M. Cho, Texas A&M Univ.

Fine Mode - Radiance

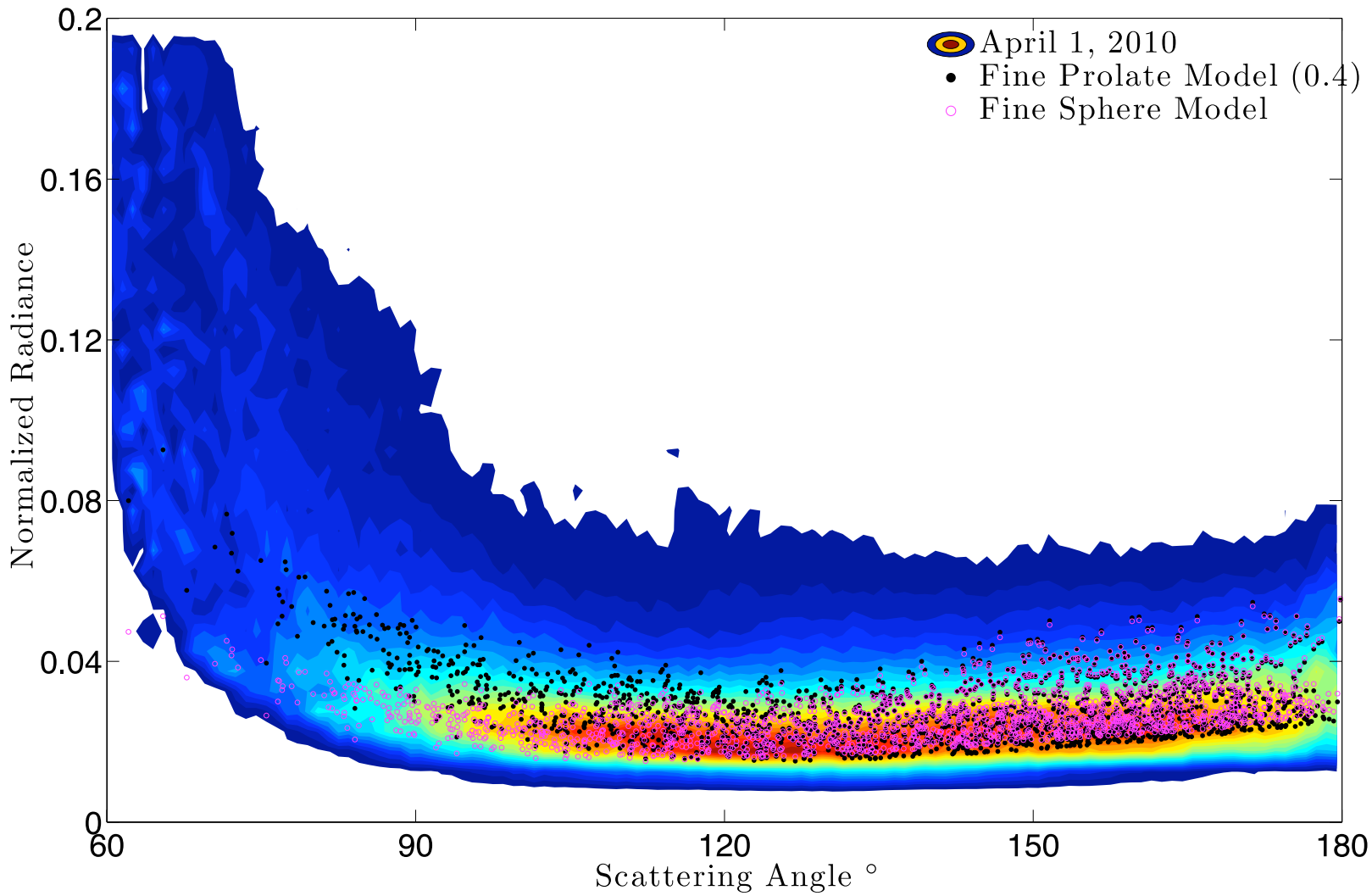

Fine Mode - Polarization

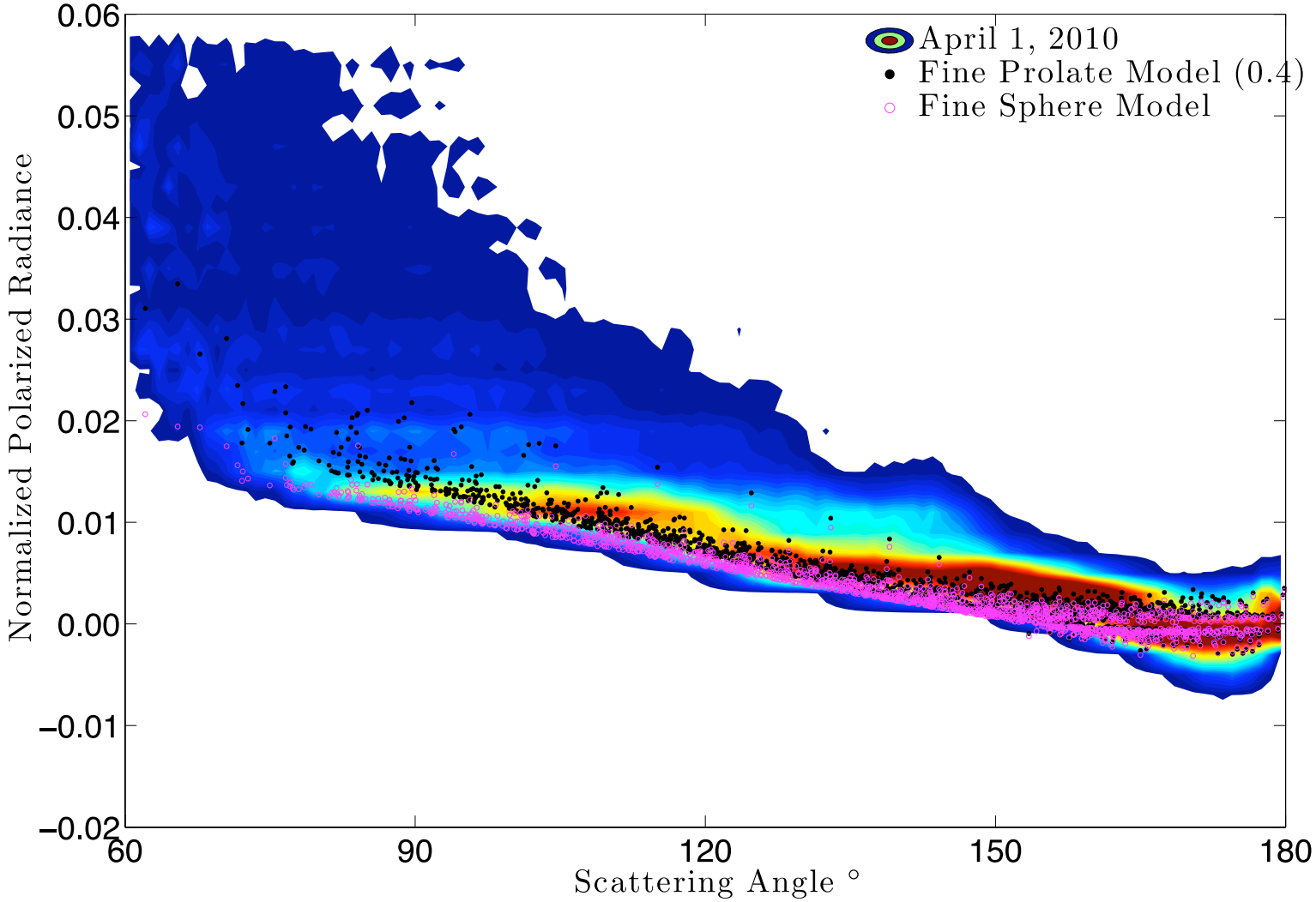

Coarse Mode - Radiance

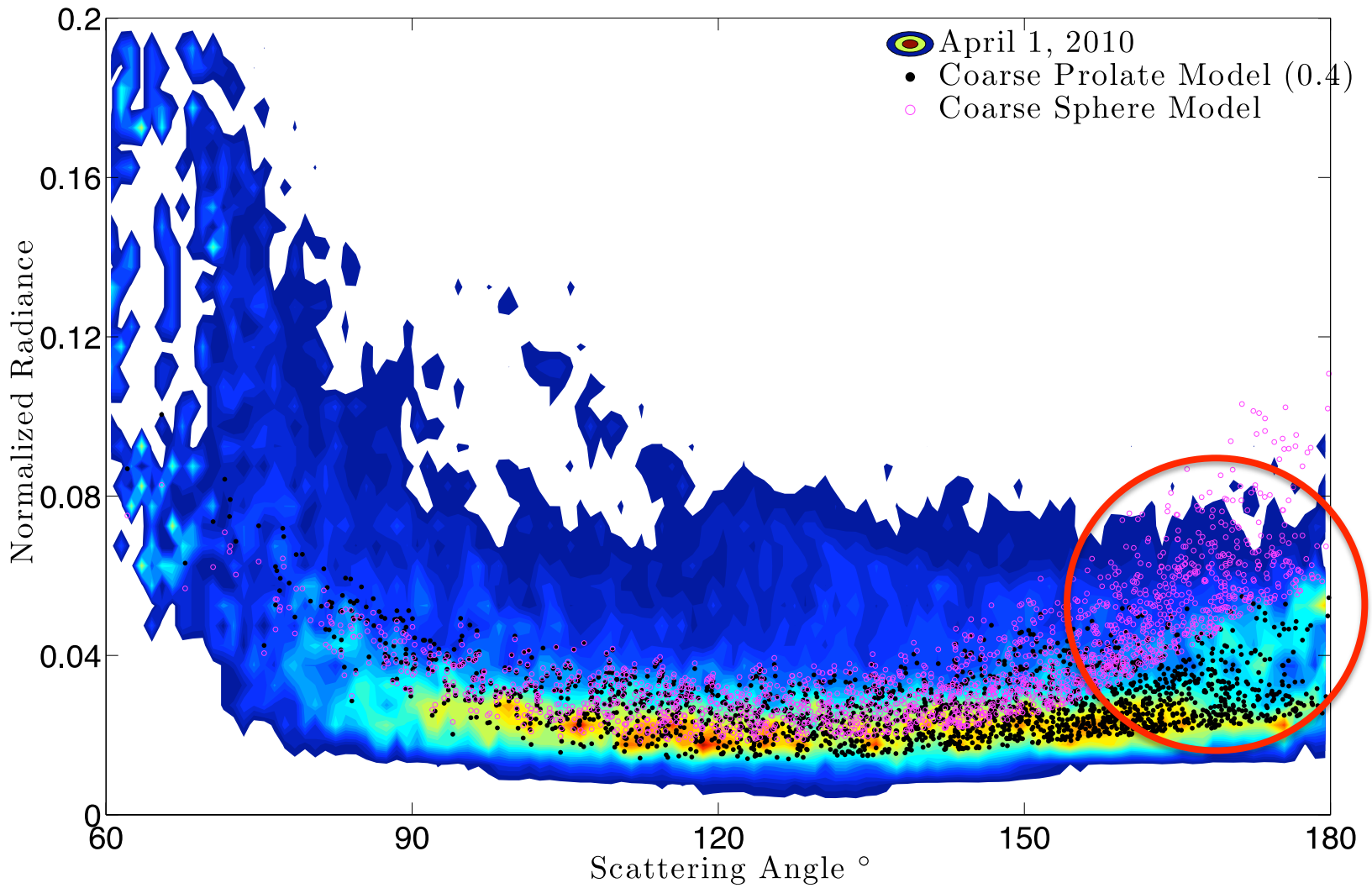

Coarse Mode - Polarization

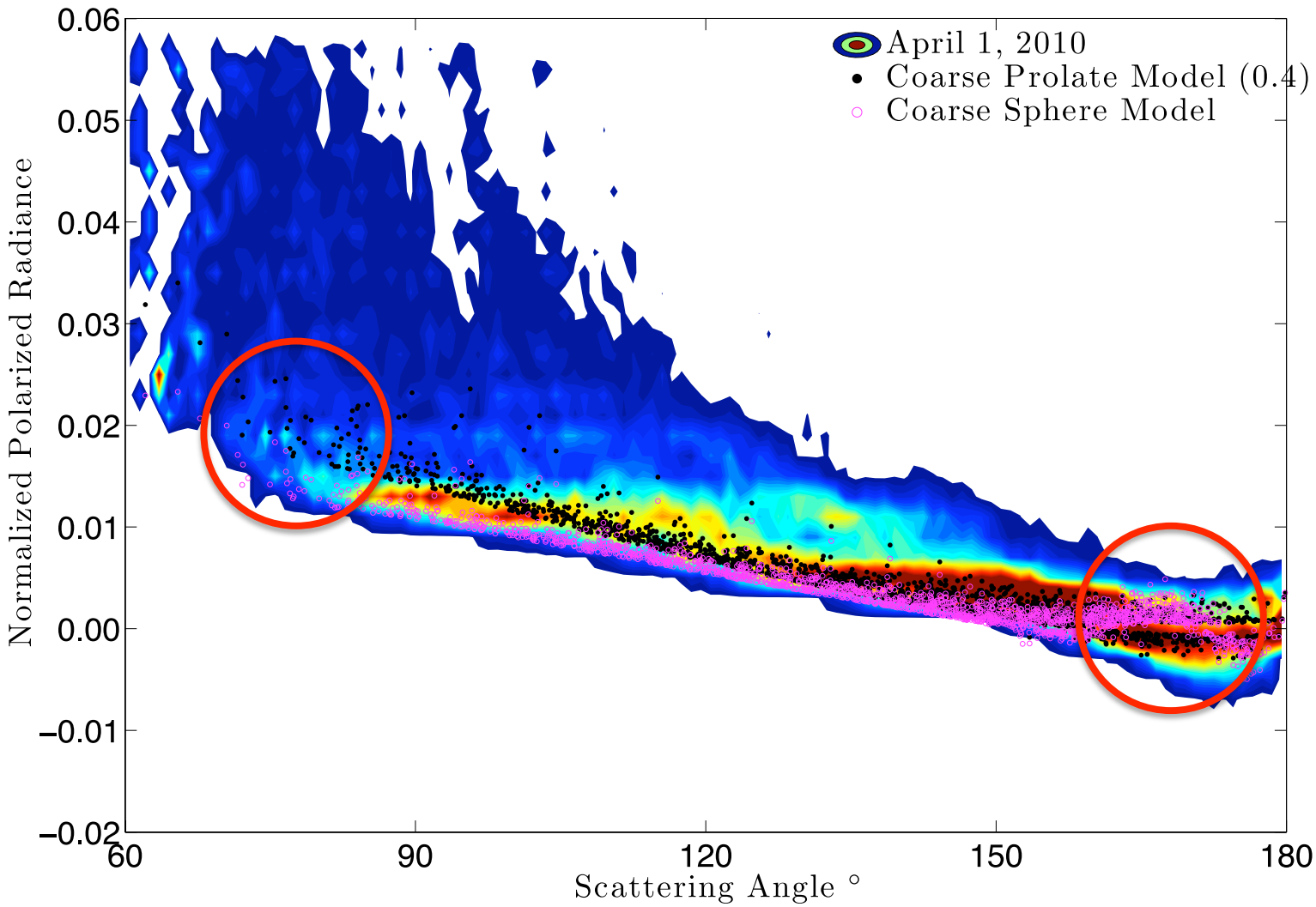

Preliminary Results (over Land)

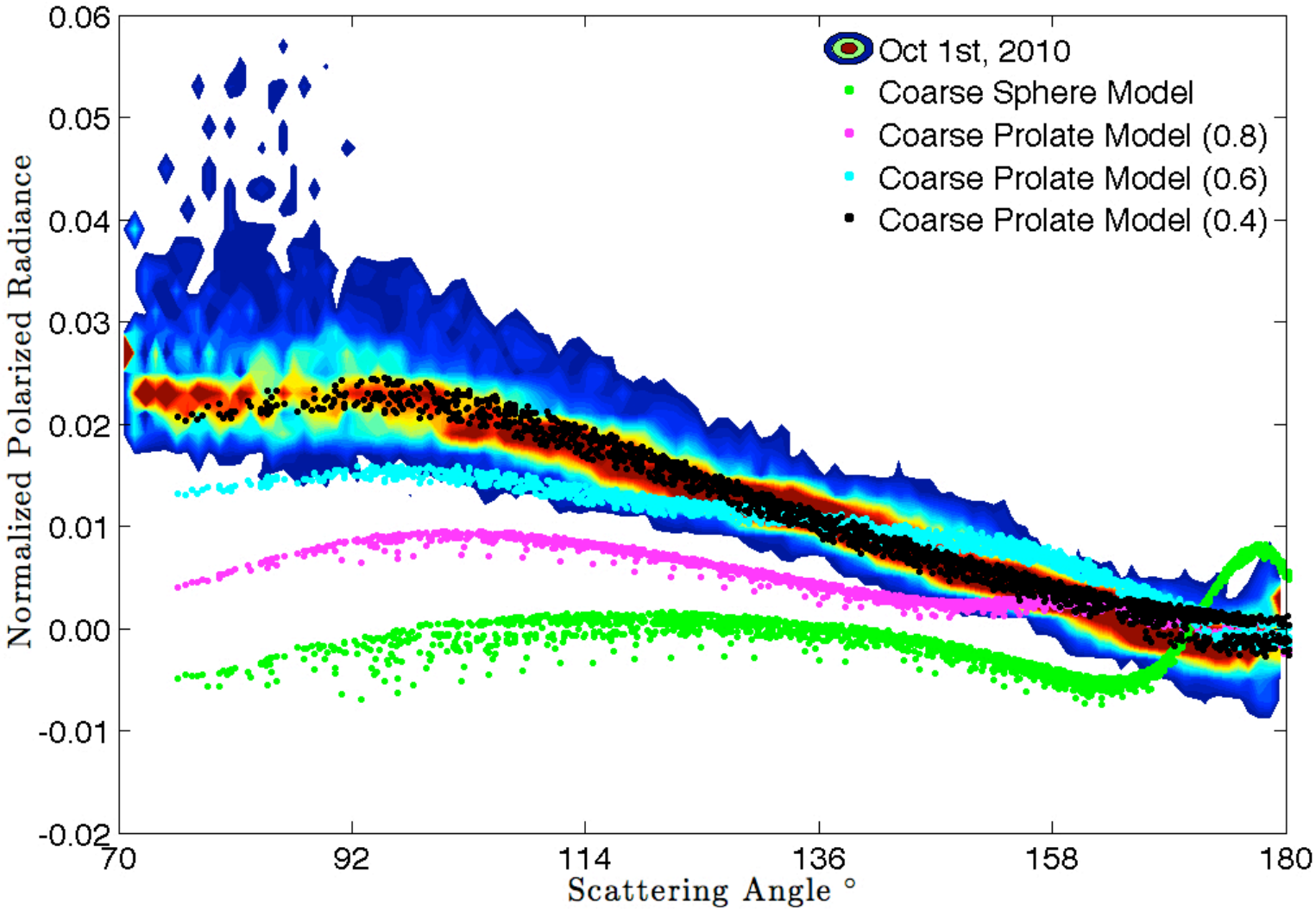

The *δ-γ'* relationships for different aerosol types

6 aerosol types: the integrated attenuated backscatter, the particulate depolarization ratio, surface types, and layer elevation

2008

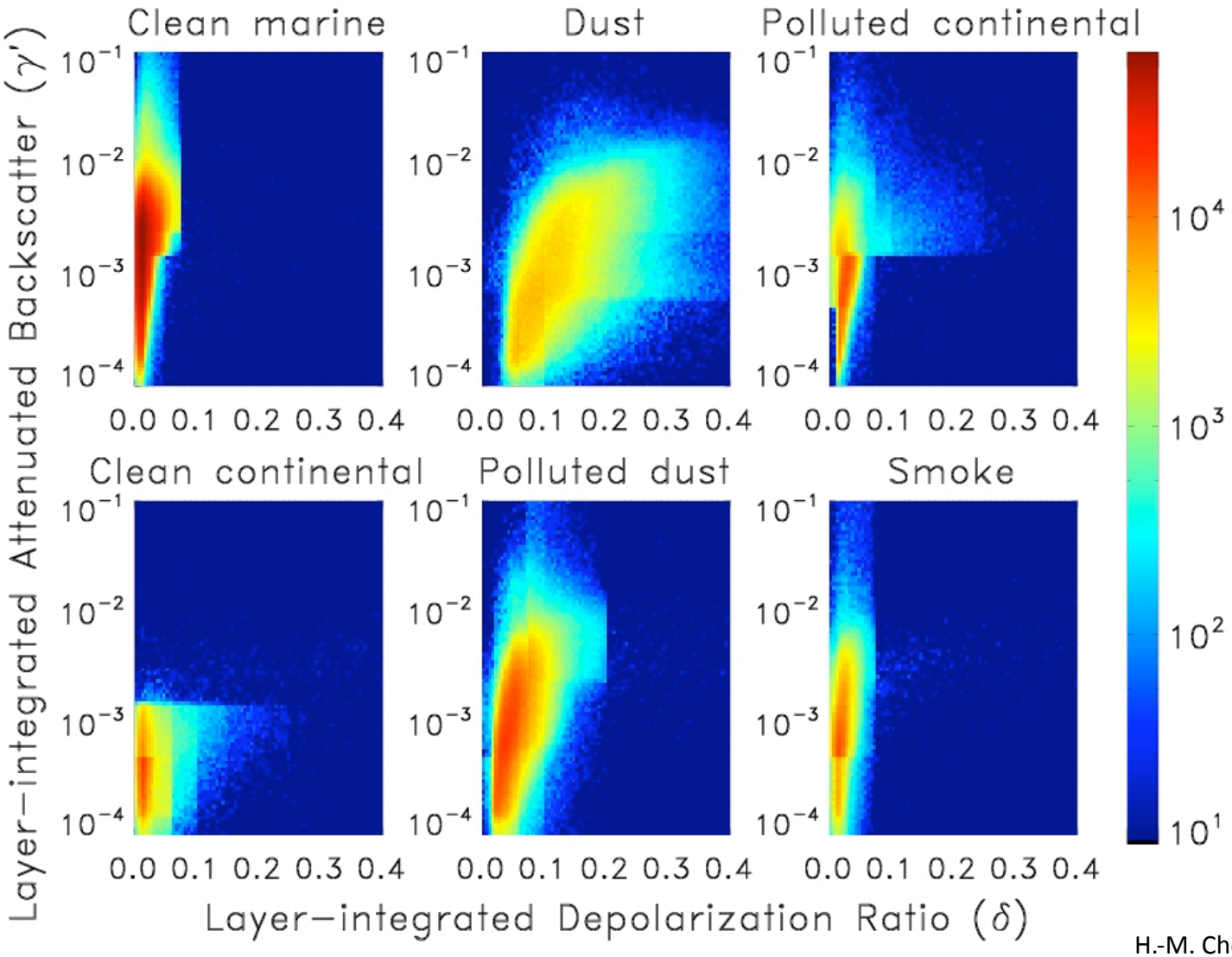

H.-M. Cho, Texas A&M Univ.

Summary

- The effect of particle nonsphericity on dust radiative properties is significant from both remote sensing and radiation budget perspectives.

- The degree of particle nonsphericity is specified in terms of the aspect ratio.

- Using POLDER data, we illustrated that, for fine mode aerosols, the effect of particle nonsphericity is not pronounced over ocean when the optical depth of an aerosol layer is very small; however, for coarse mode dust particles, the spherical model may cause large errors.
- The preliminary results for dust over land indicate that dust particles are highly nonspherical with a mean aspect ratio of approximately 0.4.

- The CALIPSO-CALIOP observations (specifically, the relation between the backscatter and depolarization ratio) can be used to constrain the determination of the particle aspect ratio.